Applied Surface Science Advances 32 (2026) 100947

Contents lists available at ScienceDirect

Applied Surface Science Advances

journal homepage: www.sciencedirect.com/journal/applied-surface-science-advances

Periodic surface structure formation on silicon surfaces by irradiation of single and multiple femtosecond laser pulses

Iaroslav Gnilitskyi [a,b,c,*], Oksana Chukova [d,e], Arno Jeromin [f], Thomas F. Keller [f,g], Tzveta Apostolova [h,i,*]

[a] Department of Physics and London Centre for Nanotechnology, King's College London, London, United Kingdom
[b] NoviNano Lab LLC, 79000, Lviv, Ukraine
[c] Department of Applied Physics and Nanomaterials Science, Lviv Polytechnic National University, 79013, Lviv, Ukraine
[d] Deutsches Elektronen-Synchrotron DESY, Notkestr. 85, 22607 Hamburg, Germany
[e] Taras Shevchenko National University of Kyiv, Volodymyrska, 60, 01601, Kyiv, Ukraine
[f] Centre for X-ray and Nano Science CXNS, Deutsches Elektronen-Synchrotron DESY, Notkestr. 85, 22607 Hamburg, Germany
[g] University of Hamburg, Department of Physics, Notkestraße 9-11, 22607 Hamburg, Germany
[h] Institute for Nuclear Research and Nuclear Energy, Bulgarian Academy of Sciences, 72 Tsarigradsko shausse, Sofia, Bulgaria
[i] Institute for Advanced Physical Studies, New Bulgarian University, 1618 Sofia, Bulgaria

ARTICLE INFO

Keywords:
LIPSS
ultrashort laser pulse
first-principles calculations
Si substrates
surface plasmon polaritons

ABSTRACT

Laser-induced periodic surface structures (LIPSS) were fabricated on silicon substrates using a low number of ultrashort laser pulses with 266 fs pulse duration at a 1030 nm wavelength. The obtained structures were investigated with SEM and EDX techniques, then the obtained results were simulated by theoretical calculations. In the applied theoretical approach, the LIPSS formation is simulated by a semi-empirical model of interference of the incident laser beam with surface-scattered electromagnetic waves generated at a rough surface, which includes excitation of surface plasmon polaritons (SPP) and accounts for the transient intrapulse changes in optical properties due to photo-excitation of a dense plasma of electron-hole pairs. The threshold conditions for SPP excitation were shown to depend on the laser fluence, wavelength, polarization, and number of pulses. These thresholds were determined from first-principles calculations of the macroscopic dielectric function of the photoexcited material.

The theoretical simulations demonstrate good agreement with the experimental observations obtained from SEM analysis. In particular, the optimal number of laser pulses required to achieve the highest LIPSS periodicity was determined to be two pulses from the theoretical model and three pulses from the experimental study. The corresponding LIPSS periods were found to be 0.922λ and 0.93λ, respectively. Overall, the applied theoretical framework shows strong consistency with experimental results and can be further used for predictive optimization of LIPSS formation conditions for different laser parameters.

1. Introduction

Laser induced periodic surface structures (LIPSS) formation is a universal phenomenon characterized by threshold behavior [1,2]. LIPSS can be successfully created using ultrashort laser pulses. While processing speed varies with average power, the use of nanosecond pulsed lasers can be cost-effective solution and reduce processing time, especially for large-surface processing industry needs. Usually, LIPSS imprinting on material surfaces is performed by laser pulses with relatively low laser fluences, near or only slightly above the ablation threshold [3–5]. This requires dozens or even hundreds of laser pulses coupled dozens, or even hundreds, of laser pulses focused on the same spot to the same irradiation spot on the surface to produce the periodic surface relief. It has long been assumed that increasing the laser fluence well above the ablation threshold would result in disordering, or even the complete erasure, of the periodic structures due to the recoil pressure of the ablation plume [6]. Recently, an alternative, more advanced method for the fabrication of nanostructures was proposed [7,8]. This method employs femtosecond laser pulses in a single-step process, enabling the formation of high-quality nanostructures.

* Corresponding authors.
E-mail addresses: iaroslav.gnilitskyi@kcl.ac.uk (I. Gnilitskyi), tzveta.apostolova@nbu.bg (T. Apostolova).

https://doi.org/10.1016/j.apsadv.2026.100947
Received 27 July 2025; Received in revised form 25 January 2026; Accepted 3 February 2026
Available online 18 February 2026

The formation of LIPSS has been studied over a broad range of wavelengths and pulse durations on different materials including metals [9], semiconductors [10], dielectrics [11], and polymers [12]. LIPSS formed on different materials can be used as a method to control and change surface characteristics in various scientific, biomedical, and industrial applications [13–16]. The most commonly accepted mechanism of LIPSS formation is associated with the interference of incident laser light with a wave propagating along the surface, leading to a periodic intensity modulation that is imprinted onto the surface of the material [17]. Based on their spatial periodicity, LIPSS formed in the ablation regime are generally classified into two main types: low-spatial-frequency LIPSS (LSFL), characterized by a period comparable to the laser wavelength, and high-spatial-frequency LIPSS (HSFL), whose period is typically an order of magnitude smaller than the laser wavelength [18]. The formation of HSFL has been successfully described by numerical solutions of Maxwell's equations[19]. An alternative theoretical approach suggests that laser irradiation induces a softening of crystal bonds, leading to an unstable molten surface layer that undergoes self-organization during re-solidification and forms periodic surface structures [20]. Recent studies, however, have demonstrated that high-quality periodic nanostructures can be achieved not only via single-step approaches, but also by employing ultrashort laser irradiation with a low number of pulses [14–17]. These results indicate that the interplay among laser fluence, pulse number, and material response is significantly more complex than previously assumed, thereby opening new opportunities for efficient, scalable nanostructuring. Nevertheless, the mutual influence of these parameters and their combined role in LIPSS formation remain under active discussion.

In this work, we systematically investigate the effect of the number of laser pulses on the formation, morphology, and quality of LIPSS, with particular emphasis on regimes ranging from single-pulse irradiation to multi-pulse exposure. By combining experimental observations with theoretical analysis, we aim to clarify the conditions required for stable periodic structure formation and to identify processing windows that enable high-quality LIPSS fabrication using a reduced number of laser pulses. We describe LIPSS periodicity using a theoretical model that accounts for transient intrapulse changes in optical properties due to photoexcitation of a dense plasma of electron-hole pairs and for the excitation of surface plasmon polaritons (SPPs). The threshold for SPP excitation depends on the laser energy flux, wavelength, polarization direction, and pulse number. We determine these thresholds from the first-principle calculation of the macroscopic dielectric function of a photoexcited solid and compare with the experimental results obtained by SEM imaging. The obtained results provide important insights for the optimization of laser-based surface structuring technologies and their practical implementation in scientific and industrial applications. From an industrial perspective, the ability to form high-quality LIPSS with only a few laser pulses is particularly important. Reducing the required pulse number directly translates into higher processing speeds, lower energy consumption, and improved throughput, which are critical factors for large-area and high-volume surface processing. Such low-pulse-number regimes enable efficient implementation of laser surface structuring using high-repetition-rate ultrashort laser systems and facilitate scaling toward industrial manufacturing.

2. Methods

Laser surface structuring of silicon was performed using a Light Conversion femtosecond laser system (Pharos) operating at a central wavelength of 1030 nm with a pulse duration of 266 fs. The laser fluence was fixed at 0.5 J cm^{-2} and the repetition rate at 1 kHz, while the number of pulses incident on a single irradiation spot was varied from 1 to 10. The focused laser beam diameter was 10.38 μm ($1/e^2$). A detailed calculation of the focused laser spot size was performed in the MAPLE experiments, including all relevant optical parameters, to ensure full clarity and reproducibility.

Prior to laser processing, silicon samples were cleaned sequentially in acetone, isopropanol, and deionized water using ultrasonic agitation for 10 min in each solvent, followed by drying in a nitrogen flow. The samples were then mounted on a motorized translation stage and irradiated under ambient atmospheric conditions at room temperature. For silicon irradiated with ultrashort pulses at 1030 nm, literature reports a single-pulse ablation/modification threshold around ~0.43 J/cm^2, i.e., within the 0.4–0.5 J/cm^2 range depending on the surface/oxide condition and threshold criterion [18–20]. Importantly, the fluence window used in the present study was chosen in line with our previous work on silicon (Gnilitskyi et al. [7]), where highly-regular LIPSS (HR-LIPSS) were demonstrated to form in the strong-ablation regime at fluences significantly above the ablation threshold, which is essential for achieving high regularity and process stability. After laser treatment, the samples were gently rinsed with isopropanol to remove loose debris and dried in nitrogen. No additional surface coating was applied prior to microscopy in order to preserve the native surface morphology.

The surface microstructure and chemical composition of the processed samples were examined using a high-resolution field-emission scanning electron microscope (FE-SEM, Nova NanoSEM 450, FEI Thermo Fisher Scientific) [21]. Secondary electron images were acquired at accelerating voltages of 5 kV and a working distance of 5–8 mm to ensure high surface sensitivity and spatial resolution. Energy-dispersive X-ray spectroscopy (EDX) was employed for elemental analysis, using an attached X-Max 150 EDX silicon drift detector with an energy resolution of 127 eV @ MnKα (Oxford). The EDX spectra were collected at an accelerating voltage of 5 kV.

Calculations of spectral properties were carried out using a theoretical model that describes transient intrapulse changes in the optical properties of silicon due to photoexcitation of a dense plasma of electron-hole pairs, including excitation of surface plasmon polaritons (SPP). Details of the theoretical approach and methodology can be found in Refs. [6]' [22], where the time-dependent Schrödinger equation for band gap materials irradiated by a linearly polarized intense ultrashort laser pulse with near-infrared wavelength is solved numerically. The method has been theoretically and computationally modified recently to describe appropriately the interaction of mid infrared laser pulses with semiconductor materials. The time-dependent electric field of the transmitted pulse is given by

$$\vec{E}(t) = \vec{E}_{ext}(t) + \vec{E}_{ind}(t) \quad (1)$$

where the induced electric field $\vec{E}_{ind}(t)$ accounts for the macroscopic polarization of the material and the applied electric field has a Gaussian temporal profile.

$$\vec{E}_{ext}(t) = \vec{e}\exp\left[-\ln 4t^2 / \tau_L^2\right] F\cos\omega_L t \quad (2)$$

Here $\vec{e}$ is a unit vector in the direction of the laser polarization, ω_L is the laser frequency corresponding to the photon energy, $\hbar\omega_L = 1.23eV$, τ_L is the pulse length, and F is the electric field strength.

3. Results and discussion

3.1. Microstructure of the created dots

The SEM investigation of the studied samples has confirmed the formation of the periodic structures under laser pulses. A panoramic SEM image of the series of LIPSS dots created on the silicon surface under irradiation with linearly polarized femtosecond laser pulses (266 fs) with the same fluence and different numbers of laser pulses (N = 1,2,3,5,7,10) is shown in Fig. 1. The dots for each of the noted numbers of pulses were created 5 times. The first and most important result demonstrated here is a very good reproduction of the visually observed properties of the created dots as a function of the number of pulses. This result indicates that we can create LIPSS dots on silicon surfaces with

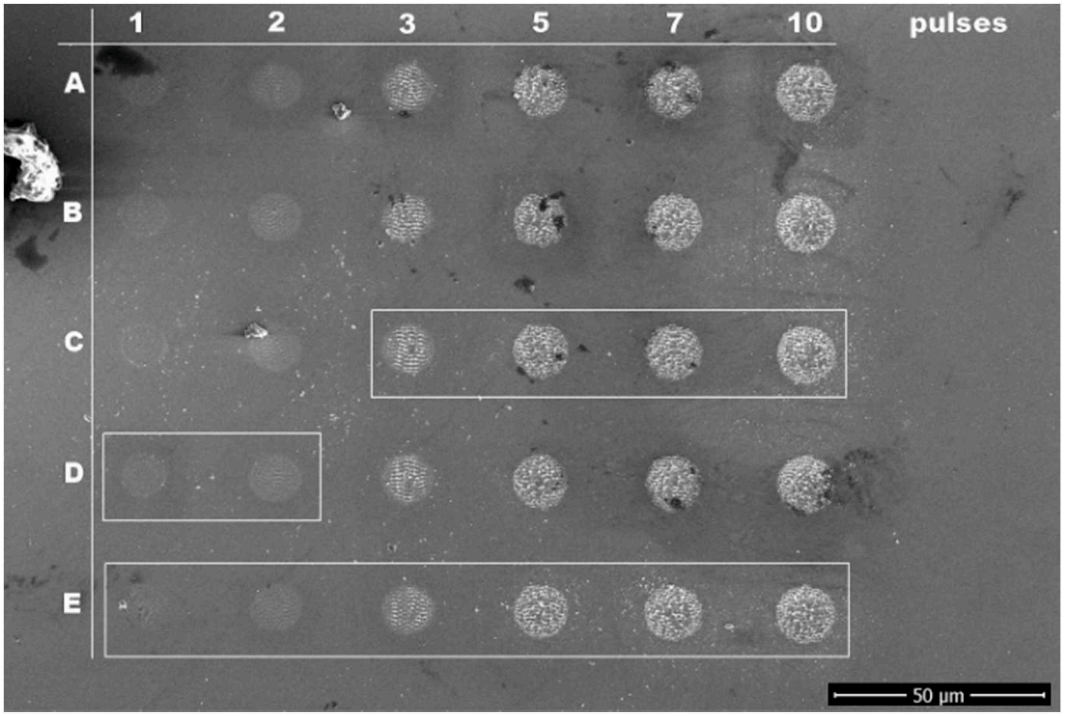

Fig. 1. Panoramic SEM image of the series of LIPSS dots created on the silicon surface under irradiation with linearly polarized femtosecond laser pulses (266 fs) with the same fluence and different laser pulses (N = 1, 2, 3, 5, 7, and 10) as noted at the top of the image. Letters at the left mark rows of the same consequent attempts repeated by identical settings.

reproducible, predictable characteristics under the proposed experimental conditions. The second important result is that the structure and dimensions of the created dots depend on the number of pulses. In the latter case this is a weak effect: diameters of the dots slightly depend on the number of pulses and increased from 10.4 microns for the dots obtained with 1 pulse to 14 microns for the dots obtained with 10 pulses that is in good agreement with the 10.4 microns diameter of the applied focused laser beam (Fig. 1). The structure of the created dots is considered for each number of pulses in more details below. For this consideration, we choose the two most successful attempts for each number of pulses.

The SEM images of dots created with a single pulse shot are shown in Fig. 2, dots D1 and E1. As it is possible to see here, the single pulse shot with applied parameters did not lead to the appearance of well-recognized periodic surface structures, but a trace of the laser pulse can be clearly seen on the SEM images even for the single pulse shots (Fig. 2). The dots have distinctive round borders, and they are surrounded by a cycle of a lighter area with 0.5-micron width (Fig. 2, a, dots D1 and E1). The diameters of the dots taken into the inner borders are 10.5 and 10.4 microns for the D1 and E1 dots, respectively.

A distinctive periodicity of the structure of the created dots is appearing with 2 pulses (Fig. 2, dots D2 and E2). One can see well-separated periodical horizontal rows with only lightly revealed periodicity inside each of these rows. The horizontal rows have a width of around 0.9 micron with interval spaces around 0.1 micron between rows. The structured round areas have well recognized unstructured borders. The diameters of the structured round areas are 11.8 and 11.0 microns for the D2 and E2 dots, respectively. Widths of the borders are 0.6 and 0.9 microns for the D2 and E2 dots, respectively.

The best LIPSS were obtained with 3 laser pulses (Fig. 2, dots C3 and E3). Their periodicity is around 0.96 microns, equal to 0.93λ, where λ is the laser wavelength. The horizontal rows also exhibit periodic properties. Their widths and margins are changing by about 0.5±0.2 microns. The widths are not constant; they vary within the noted margins with a periodicity of 1 micron. Dimensions of the LIPSS area are 12 microns for the C3 and E3 dots, and the border widths are around 0.6 microns. Most of the LIPSS dots created with 3 pulses exhibit defects in their periodicity at their centers (Fig. 1). Some evidence of the formation of deeper structural levels with a similar periodicity can be seen in these LIPSS in high-resolution images (Fig. 2, dot E3).

Images of the LIPSS created with 5 laser pulses have clearly revealed formation of a deeper layer and even of periodicity in the third direction (Fig. 2, dots C5 and E5). However, the periodicity of these samples is not very good. The damaged central area is more spread. Only some places between centers and borders can still demonstrate good periodicity. Despite this, the period of structure repetitions is the same for all the places where it is possible to define it exactly, and it is around 1 micron as for the previous cases. The LIPSS area is around 13 microns in diameter. The borders observed for the dots created with a lower number are already covered by the structured area for the LIPSS created with 5 pulses, but they can still be seen in Fig. 2, dots C5 and E5. For the LIPSS created with 7 and 10 pulses, the borders are not observed, diameters of the LIPSS areas are 13.5 and 14 microns, respectively (Figs. 2, dots C7 and C10). The quality of periodicity also decreases with increasing the number of pulses to 7 and 10, but this decrease is not as distinct as it was between the LIPSS created with 3 and 5 pulses. The periodicity of the structures is also around 1 micron.

Thus, the quality of the LIPSS dots produced depends strongly on the number of pulses. The most favorable number of pulses for creating LIPSS on silicon surfaces is 3 under the pulse conditions applied here. On the other hand, the periodicity of the created structures does not depend on the number of pulses. It is always around 1 micron, which can be clearly estimated in both the horizontal and vertical directions. One can suppose that the observed 1-micron average value of repetitions can be induced by the 1030 nm wavelength of the applied laser pulses. These assumptions will be considered below in relation to the experimental and theoretical investigation of laser-induced processes on silicon surfaces that could be responsible for the formation of periodic surface structures during laser pulses.

Investigation of the elemental composition of the LIPSS profiles has

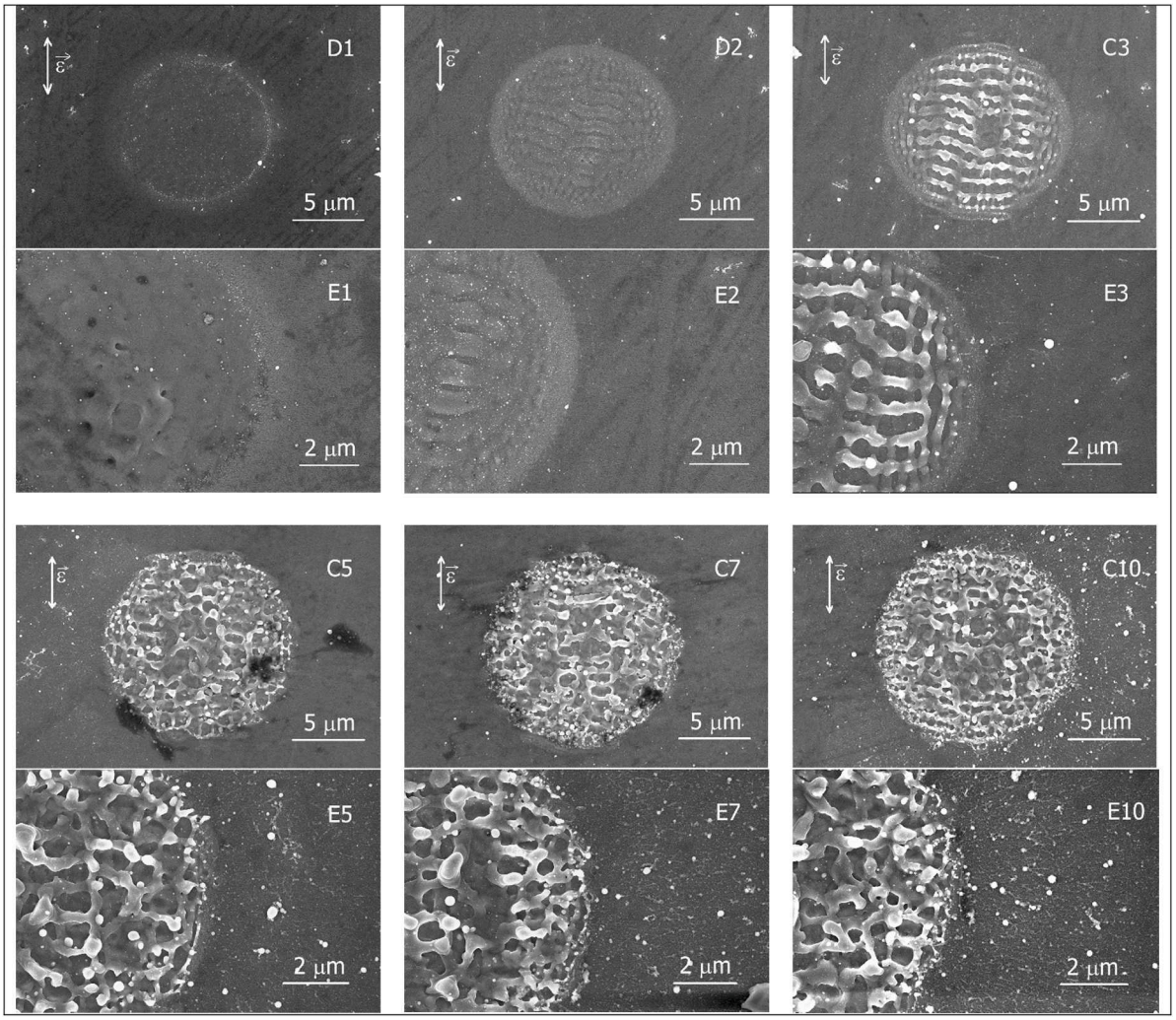

Fig. 2. SEM images of the D1, E1, D2, E2, C1, E3, C5, E5, C7, E7, C10 and E10 dots (see Fig. 1 for reference details).

shown that centers of the LIPSS units are saturated with carbon and oxygen. The process is accompanied by a decrease in the content of Si atoms at the tops, whereas between the LIPSS centers, silicon remains the main chemical element (Fig. 3).

Deviations of the chemical composition in the LIPSS are completely related to the quality of the created dots and have the same dependency on the number of laser pulses. The best results are obtained with dots created from 3 laser pulses, where the periodicity of the elemental composition is very good. The observed changes in elemental composition should affect at least the conductivity and optical properties of the created LIPSS.

3.2. *Transient Optical properties of laser-excited silicon*

The frequency-dependent dielectric function $\varepsilon(\omega)$, calculated from first principles by solving the time-dependent Schrödinger equation (TDSE) for the laser-driven solid [6], serves as the foundational quantity for our analysis. The dielectric function is derived from the non-equilibrium distribution of conduction electrons following photoexcitation, which is highly non-uniform and anisotropic across the Brillouin zone. This first-principles approach contains no fitting parameters; the optical response is computed directly from the microscopically derived carrier distributions.

Using these calculated distributions, the complex optical constants were simulated. The resulting $\varepsilon(\omega)$ represents the electromagnetic response of the material in the specific, nonlinearly generated state. This provides a fundamental advantage: while the real part of the dielectric function for photoexcited silicon can be phenomenologically fitted with a Drude model using an effective mass m^* as a free parameter, such fits can yield unphysical trends. In contrast, our direct, parameter-free calculation from the anisotropic non-equilibrium distributions predicts a physically rigorous, first-principles basis for obtaining $\varepsilon(\omega)$ and correctly identifying plasmonic conditions. When a high-intensity ultrashort laser double pulse irradiates silicon, it generates dense, anisotropically distributed electron-hole plasma, transiently inducing a metallic state. This dramatically modifies $\varepsilon(\omega)$ driving $\mathrm{Re}[\varepsilon(\omega)]$ toward negative values, with the condition for supporting surface plasmon polaritons (SPPs) at the vacuum-material interface $\mathrm{Re}[\varepsilon(\omega)] < -1$. We theoretically show that, once this condition is met, SPPs are excited, leading to the formation of low-spatial-frequency LIPSS (LSFL) with periods near the laser wavelength.

The sharp plasmonic resonance threshold is rigorously defined only through this first-principles, parameter-free dielectric function. A pronounced, resonant plasmon mode requires that Re[epsilon(omega)] is sufficiently negative while $\mathrm{Im}[\varepsilon(\omega)]$ remains relatively small over a narrow bandwidth. This spectral criterion distinguishes a sharp resonance from a broad, overdamped excitation. Consequently, the effective plasma frequency ω_p is not a fitted parameter but is self-consistently determined by the dielectric function (via the condition $\mathrm{Re}[\varepsilon(\omega)] = 0$). The fluence threshold F_{th} for the plasmonic condition is therefore the fluence at which the TDSE-calculated $\varepsilon(\omega)$ first satisfies the combined criteria of sufficiently negative $\mathrm{Re}[\varepsilon(\omega)]$ and low loss, thereby defining

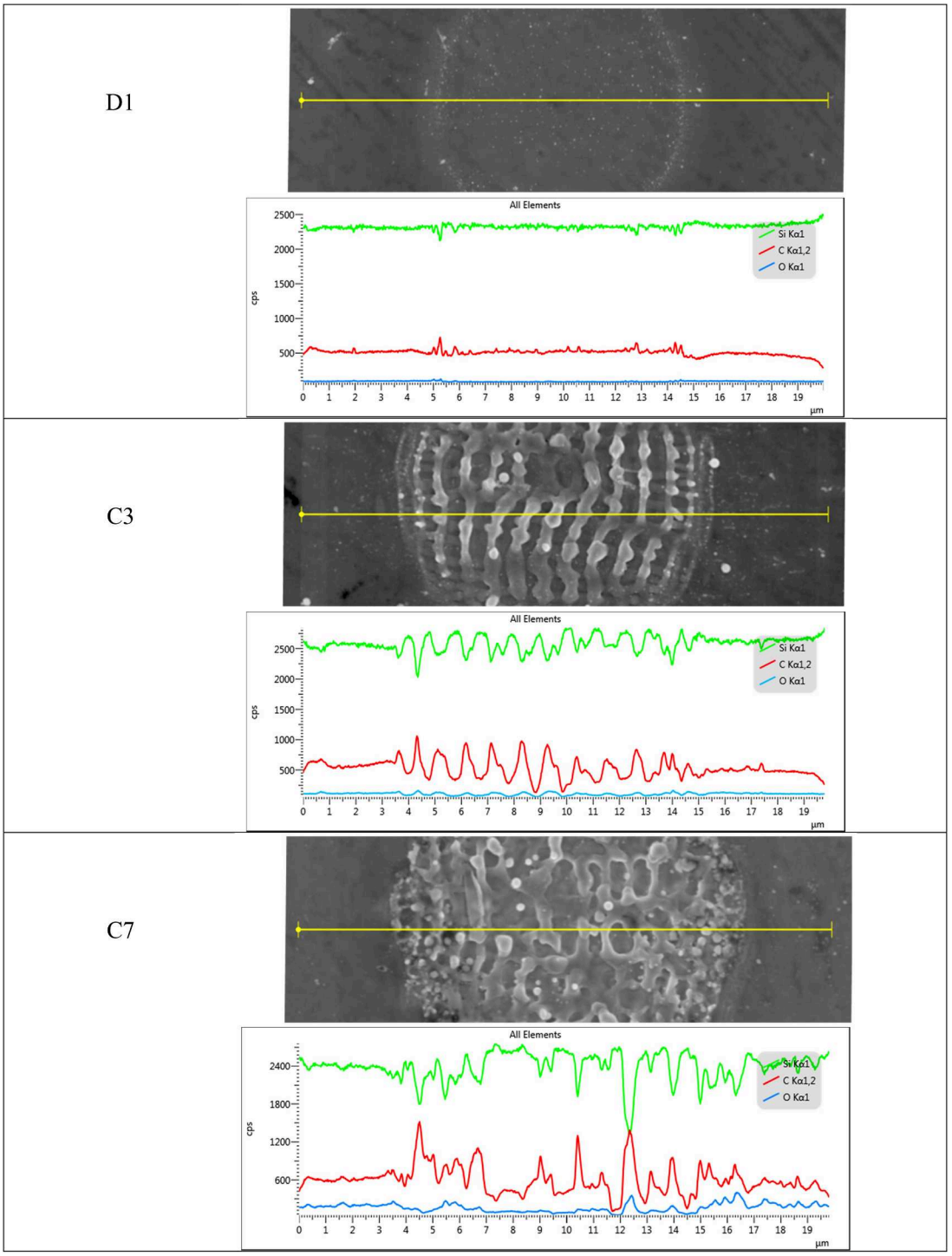

Fig. 3. EDX analysis of the dots D1, C3 and C7 (top to down). Top, SEM image with below, corresponding line profiles of Si $K\alpha_1$, C $K\alpha_2$ and O $K\alpha_1$, respectively.

the onset of a resonant plasmon in the transient metallic layer.

Thus, we theoretically study laser-induced periodic surface structures (LIPSS) with periods near the laser wavelength (LSFL $\sim \lambda_L$) or low-spatial-frequency LIPSS (LSFLs), which form in the laser-irradiated semiconductor. It becomes highly absorptive after irradiation with the double laser pulse and the LSFL on silicon are formed due to the excitation of mid-infrared- laser-wavelength SPP following the transition to quasi-free carrier generation-induced metallic state of Si under high laser intensities.

In Fig. 4 we present the real Fig. 4 (a) and imaginary Fig. 4 (b) parts of the dielectric function of the photoexcited Si for varying laser fluence of the driving femtosecond double pulse. It is observed that $\mathrm{Re}[\varepsilon(\omega, F)]$ it becomes negative for increasing laser fluence (Fig. 4(a)) due to the formation of free carrier plasma, while $\mathrm{Im}[\varepsilon(\omega, F)]$ increases below the direct absorption edge - Fig. 4 (b).

The imaginary part of the calculated dielectric function is consistent with the measured one and the direct band gap of silicon found is close to the experimentally obtained value [23]. As laser fluence increases the observed main peak in the imaginary part of the calculated dielectric function decreases and lower peaks are formed below the absorption edge, which is in good agreement with the results obtained previously from other ab initio methods [24].

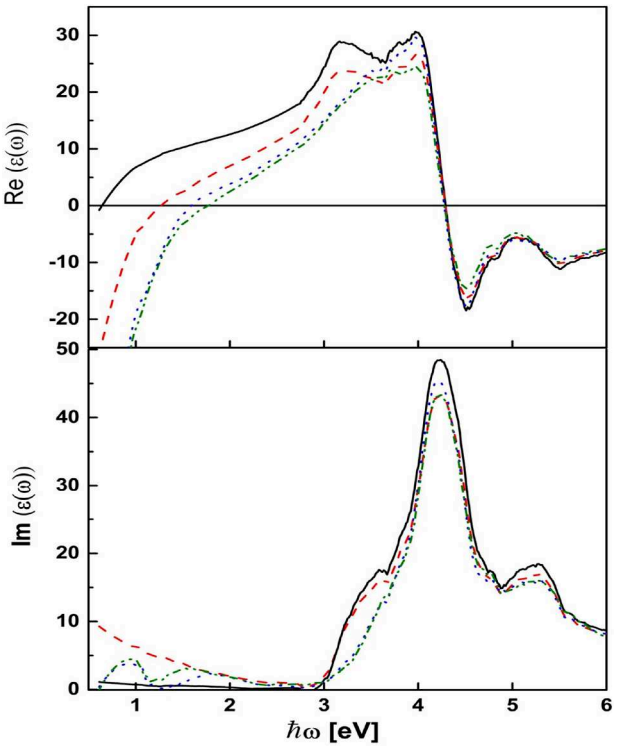

Fig. 4. Real (a) and imaginary part (b) of the transient dielectric function of Si excited by a double laser pulse of 260 fs, with wavelength of 1030 nm and linear polarizations of the laser along the [001] axis. The fluences of the applied laser field are F = 2.8 J/cm^2 (solid black curve), F = 3.8 J/cm^2 (dash red curve), F = 4.8 J/cm^2 (dot blue curve) and F = 6.4 J/cm^2 (dot-dash green curve).

Since the absorption of the femtosecond double laser pulse in silicon occurs via the generation of quasi free electrons in the conduction band of the solid on time scales shorter than the electron-phonon relaxation time, we calculate the transient absorption coefficient and reflectivity of the laser-excited silicon for the experimental conditions.

In Fig. 5 the frequency-dependent absorption coefficient $\alpha(\omega)$ (left panel) and reflectivity $R(\omega)$ for normal incidence (right panel) of the photo-excited Si are presented for varying peak laser intensities of the mid-infrared double pulse. We define the frequency-dependent absorption coefficient by $\alpha(\omega) = 4\pi\kappa/\lambda\alpha$, where κ is the extinction coefficient of the laser-excited Si and λ is the wavelength in vacuum.

For a lower laser fluence of the driving mid-infrared pulse, it can be seen from Fig. 5 (a) that the absorption coefficient $\alpha(\omega)$of silicon is primarily governed by its imaginary dielectric function Im$[\varepsilon(\omega, F)]$, which arises from interband transitions in which photons with energy greater than the bandgap excite electrons from the valence band to the conduction band.

As the laser fluence increases, the dominant absorption peak diminishes in magnitude and shifts toward higher frequencies. At the highest fluence, the double-pulse-generated plasma induces a highly absorptive state in silicon as seen in Fig. 5 (c). For $\alpha(\omega) \simeq 10^8 cm^{-1}$ in the mid-infrared spectral range.

Silicon's reflectivity transitions from dielectric-like (lower fluence) to metal-like (higher fluence) due to laser-induced carriers and nonlinear effects as seen from Fig. 5 (d) - Fig. 5 (f).

The plasma frequency of Si excited by laser pulse with linear polarization along the [001] for $\tau = 260$ fs is plotted in Fig. 6. In this work it is not a fitted parameter but is self-consistently determined by the dielectric function via the condition Re$[\varepsilon(\omega, F)] = 0$.

3.3. Modeling the excitation of surface plasmon polaritons

To describe the excitation of SPP, dispersion relations are obtained from the continuity of the electric and magnetic fields at the interface between two semi- infinite nonmagnetic media with local (frequency-dependent) dielectric functions ε_1 and ε_2 separated by a planar interface at $z = 0$ [25]. The full set of Maxwell's equations in the absence of external sources are:

$$\begin{aligned} \vec{\nabla} \times \vec{H}_i &= \varepsilon_i \frac{1}{c} \frac{\partial \vec{E}_i}{\partial t} \\ \vec{\nabla} \times \vec{E}_{ii} &= -\frac{1}{c} \frac{\partial \vec{H}_i}{\partial t} \\ \vec{\nabla} \cdot \left(\varepsilon_i \vec{E}_i \right) &= 0 \\ \vec{\nabla} \cdot \vec{H}_i &= 0, \end{aligned} \tag{3}$$

where i = 1 for z < 0 and i = 2 for z > 0.

The solutions to the above equations are s-polarized and p-polarized electromagnetic modes, with the electric field $\vec{E}$ and the magnetic field $\vec{H}$parallel to the interface, respectively. For an ideal surface, if waves are formed that propagate along the interface, there must necessarily be a component of the electric field normal to the surface. Hence, s-polarized surface oscillations (whose electric field $\vec{E}$ is parallel to the interface) do not exist.

The solution for a wave traveling along the x-axis and a magnetic field $\vec{H}$ propagating parallel to the surface (z = 0) (p-polarized wave), with the electric and magnetic fields tailing off into the positive (z > 0) and negative (z < 0) directions, is:

$$\vec{E}_i = (E_{ix}, 0, E_{iz}) \exp(-\kappa_i |z|) \exp(i(q_i x - \omega t)) \tag{4}$$

and

$$\vec{H}_i = (0, E_{iy}, 0) \exp(-\kappa_i |z|) \exp(i(q_i x - \omega t)) \tag{5}$$

where q_i represents the magnitude of a wave vector that is parallel to the surface. From Maxwell's equations, it follows that:

$$i\kappa_1 H_{1y} = \frac{\omega}{c} \varepsilon_1 E_{1x} \tag{6}$$

$$i\kappa_2 H_{2y} = -\frac{\omega}{c} \varepsilon_2 E_{2x} \tag{7}$$

and

$$\kappa_i = \sqrt{q_i^2 - \varepsilon_i \frac{\omega^2}{c^2}} \tag{8}$$

determines the decay of the electromagnetic field with increasing distance from the surface.

The boundary conditions at the plane $z = 0$ imply that the component of the electric and magnetic fields parallel to the surface must be continuous, leading to the system of equations

$$\frac{\kappa_1}{\varepsilon_1} H_{1y} + \frac{\kappa_2}{\varepsilon_2} H_{2y} = 0 \tag{9}$$

and

$$H_{1y} - H_{2y} = 0 \tag{10}$$

The condition that this system of equations has a nontrivial solution provides the dispersion relation connecting the frequency ω of the p-polarized wave and its wavenumber κ:

$$\frac{\varepsilon_1}{\kappa_1} + \frac{\varepsilon_2}{\kappa_2} = 0 \tag{11}$$

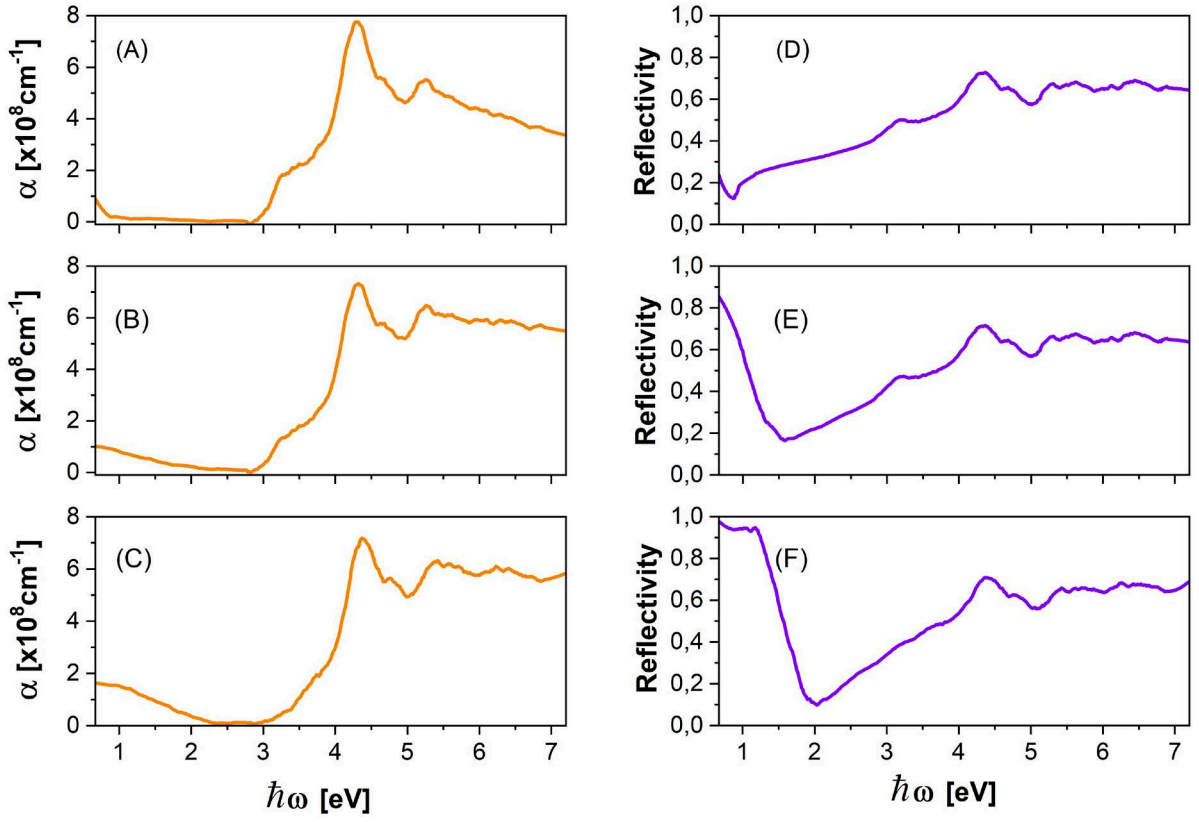

Fig. 5. Left panel- frequency dependent absorption coefficient of Si induced by a double 260 fs laser pulse with wavelength 1030 nm, linearly polarized along the [001] crystal direction. Right panel- the corresponding frequency-dependent reflectivity of photoexcited silicon. The fluence of the applied laser are 2.8 J/cm^2 (a, d), 3.8 J/cm^2 (b, e), 4.8 J/cm^2 (c, f).

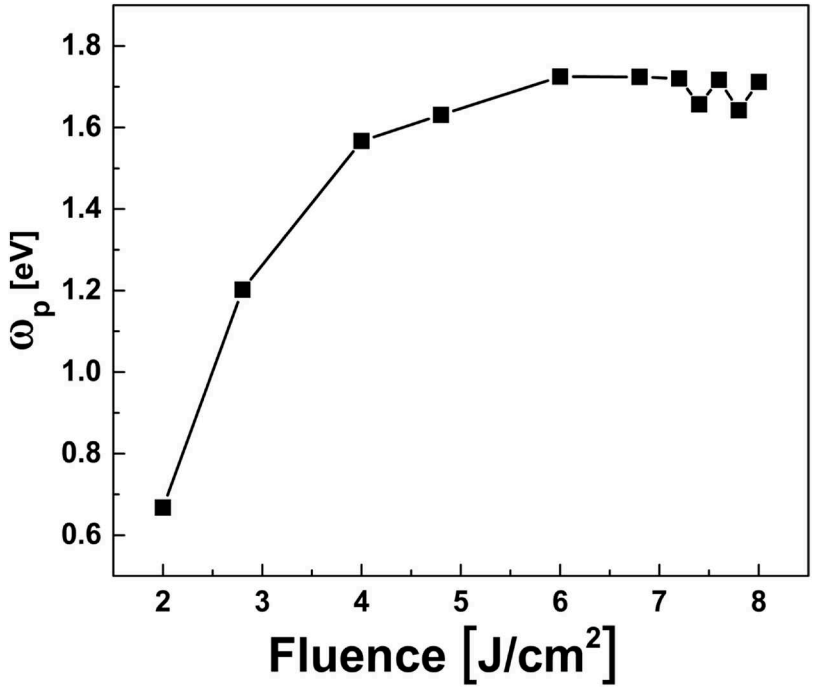

Fig. 6. Plasma frequency of Si excited by a laser pulse with linear polarization along the [001] for double pulse of $\tau = 260$ fs, and wavelength 1030 nm.

From the boundary conditions, the continuity of the wave vector in equation (8) is obtained, $q_{1x} = q_{2x} = q_x$ and therefore the SPP dispersion curve can be written as:

$$q_{sp}(\omega) = \frac{\omega}{c}\sqrt{\frac{\varepsilon_1\varepsilon_2}{\varepsilon_1 + \varepsilon_2}} \tag{12}$$

This relation is valid if ε_1 or ε_2 are complex [26] and in this case $q_{sp}(\omega)$ is also a complex wave vector whose imaginary part characterizes an exponential growth or attenuation of the SPP amplitude in its direction of propagation. There is an attenuation of SPP when$\mathrm{Im}q(\omega) > 0$.

Under the assumption that the excitation of surface plasmons and their interference with the incident beam is regarded as the predominant mechanism of periodic structure formation [27,28], the range of the computed SP wavelengths can provide an estimate of the expected subwavelength structures on the irradiated material. One way to predict the laser induced surface periodic structures (LIPSS) period in silicon is to link the SPP wavelength and the laser wavelength through the definition of the phase velocity of the SPP $v_{phSPP} = \omega/\mathrm{Re}(q(\omega))$ [29] hence the SPP wavelength is

$$\lambda_{spp}(\omega) = \frac{\omega}{c}\frac{\lambda_L}{2\mathrm{Re}(q(\omega))} = \lambda_L\sqrt{\frac{\varepsilon_1+\varepsilon_2}{\varepsilon_1\varepsilon_2}} \tag{13}$$

where $\lambda_L$is the laser wavelength? The mean free path $L_{spp}$is calculated by the imaginary part of the SPP wavenumber [30]

$$L_{spp}(\omega) = \frac{1}{2\mathrm{Im}(q(\omega))} \tag{14}$$

The SPP wavelength is directly linked to the LSFL-I periodicity ($\Lambda_{LSFL} = \lambda_{SPP}$) [31] and the SPP spatial period λ_{SPP} is related to the bulk dielectric function via equation (13).

For a small number of laser pulses, as in our case, the LSFL period may coincide with Λ SPP as the surface corrugations are still small (depths d << λ). Applying this model to semiconductors such as silicon is justified by the formation of a thin metallic layer during femtosecond laser irradiation [32]. This layer is a pseudo-metal layer formed in a solid in a regime of high electronic excitation, where resonant interband transitions occur. At high peak laser intensities, energy is still absorbed resonantly via interband transitions within the conduction band. The calculated dielectric function of the material is used to determine the fluence regime in which surface plasmon polaritons (SPPs) can form. In Fig. 4 (a), the condition for surface plasmon excitation, Re (ε) < −1[27,] is satisfied for fluences F > 2.8 J/cm^2. In this regime, we calculate the frequency-dependent SPP wavelength as shown in Fig. 7.

The SPP wavelength as a function of laser fluence is shown in Fig. 8 for a double pulse of 260 fs and a wavelength of 1030 nm. The ripple wavelength is close to the laser wavelength at higher fluences. Larger deviation from the laser wavelength occurs at the threshold fluence.

Fig. 8 shows a fluence dependent threshold to excite SP. It is seen that for a double pulse of τ = 260 fs this fluence threshold is approximately 4.8 J/cm^2. This trend agrees with the previously shown increase of optical breakdown threshold [22] with increasing pulse duration. Results presented in Fig. 8 reveal that SPP oscillations can be excited only for a certain laser fluence range, and there is a well-defined threshold fluence F_{th} for stable surface plasmon polariton excitation.

At high excitation levels, the total fluence of a double-pulse sequence, which sums the peak fluences of the individual fs-pulses [33]' can be markedly reduced due to nonlinear plasma effects, as shown explicitly [6,9]. The reduced fluence values are below the optical breakdown threshold for silicon [22] and consistent with the results for the nonlinear absorption regime [6].

Thus, the theoretically predicted ripple wavelength of 0.922λ is in very good agreement with the experimentally observed LIPSS repetition rate of approximately 0.93λ for structures created with three laser pulses. This correspondence indicates that the formed surface patterns belong to the class of low-spatial-frequency LIPSS (LSFL), which are typically characterized by periods close to the laser wavelength. At the same time, the present results clearly demonstrate that, under low-pulse-number irradiation conditions, the resulting LIPSS periodicity can be slightly smaller than the laser wavelength, reflecting the influence of transient laser–matter interaction effects and pulse-number-dependent excitation conditions. Furthermore, the optimal pulse numbers identified by theoretical modeling and experimental observations (two and three, respectively) are in close agreement, confirming the validity of the applied model. These findings provide important insight into the role of pulse accumulation effects in the early stages of periodic structure formation, demonstrating that high-quality LIPSS do not necessarily require large numbers of laser pulses. Instead, carefully controlled low-pulse-number regimes can lead to well-defined periodic nanostructures with predictable characteristics. This has direct implications for the optimization of laser surface processing, enabling a significant reduction in processing time and energy input. Overall, the good agreement between experimental results and theoretical predictions underscores the potential of the applied model as a predictive tool for tailoring LIPSS characteristics by adjusting laser parameters and pulse numbers. The outcomes of this study advance the fundamental understanding of pulse-number-dependent LIPSS formation mechanisms and offer practical guidance for efficient, scalable, and industrially relevant laser nanostructuring, particularly in applications requiring high throughput and large-area surface processing.

4. Conclusions

In this work, the formation of laser-induced periodic surface structures (LIPSS) on silicon substrates was systematically investigated using a low number of ultrashort laser pulses. By varying only the number of femtosecond pulses while keeping all other laser parameters constant,

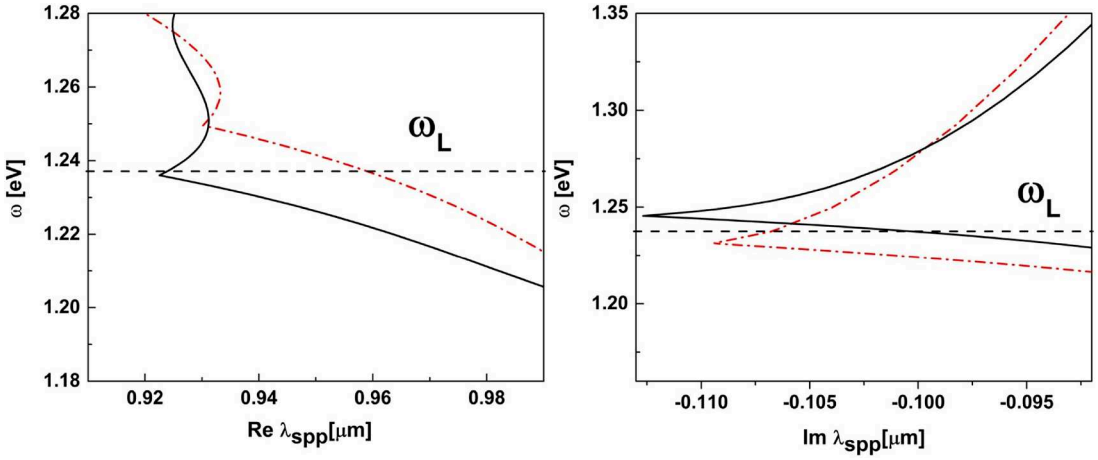

Fig. 7. Surface plasmon polariton wavelength for Si as a function of laser intensity for laser fluences F = 4.8 J/cm^2 (black solid curve) and F = 6.4 J/cm^2 (red dashed curve) for double pulse laser irradiation with duration 260 fs, wavelength 1030 nm and laser polarization along the [001] axis.

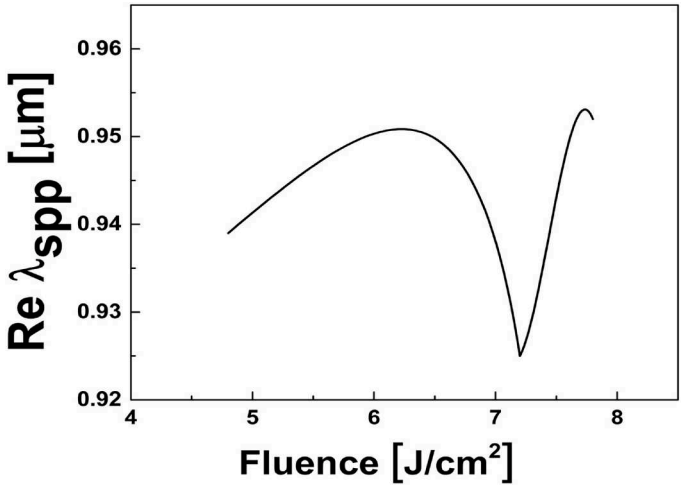

Fig. 8. Calculated surface plasmon wavelengths for Si as a function of laser fluence for laser irradiation with double pulse duration of 260 fs along the [001] axis.

the influence of pulse number on the morphology, periodicity, and quality of the resulting surface structures was clearly demonstrated. SEM analysis of the experimental results shows that single-pulse irradiation is insufficient for forming well-defined LIPSS, resulting in poorly developed, weakly ordered surface morphologies. In contrast, stable, highly periodic structures emerge when two to three laser pulses are applied, indicating an optimal low-pulse-number regime for LIPSS formation on silicon. Further increases in pulse number do not significantly improve structural quality, underscoring the importance of precise control over pulse accumulation effects.

The experimental observations were supported by theoretical simulations based on a semi-empirical interference model that accounts for surface-scattered electromagnetic waves, the excitation of surface plasmon polaritons, and transient intrapulse changes in the optical properties of silicon due to the formation of a dense electron–hole plasma. The applied theoretical approach found that the threshold for SPP excitation depends on laser fluence, wavelength, polarization direction, and pulse number. We determine these thresholds from a first-principles calculation of the macroscopic dielectric function of the photo-excited solid. The theoretical approach successfully predicts the threshold conditions for SPP excitation and reproduces the experimentally observed LIPSS periods with good accuracy. The optimal pulse numbers determined by theory and experiment (two and three pulses, respectively) show close agreement, as do the corresponding LIPSS periods (0.922λ and 0.93λ).

Overall, the good consistency between experimental and theoretical results confirms the validity of the applied model and demonstrates its potential as a predictive tool for optimizing laser-processing conditions. The findings of this study contribute to a deeper understanding of pulse-number-dependent mechanisms in LIPSS formation and provide practical guidelines for efficient, low-pulse-number laser surface structuring, which is particularly relevant for high-throughput and large-area industrial applications.

CRediT authorship contribution statement

Iaroslav Gnilitskyi: Writing – original draft, Methodology, Investigation, Conceptualization. **Oksana Chukova:** Writing – review & editing, Writing – original draft, Methodology. **Arno Jeromin:** Validation, Resources, Formal analysis, Data curation. **Thomas F. Keller:** Writing – review & editing, Visualization, Validation, Supervision, Resources, Funding acquisition, Formal analysis, Data curation. **Tzveta Apostolova:** Writing – review & editing, Writing – original draft, Visualization, Software, Methodology, Investigation, Conceptualization.

Declaration of competing interest

The authors declare that they have no known competing financial interests or personal relationships that could have appeared to influence the work reported in this paper.

Acknowledgments

Supported by the European Union within the Project 101120397 — APPROACH. The authors acknowledge DESY (Hamburg, Germany), a member of the Helmholtz Association HGF, for the provision of experimental facilities. Parts of this research were carried out at DESY NanoLab facilities. Oksana Chukova acknowledges MSCA4Ukraine project Proposal ID 1233117, which is funded by the European Union. This material is based upon work supported by the Air Force Office of Scientific Research under award number FA8655-24-1-7014 and KP-06-COST/26 (BNSF) is acknowledged (T.A.)

Data availability

Data will be made available on request.

References

[1] M. Birnbaum, Semiconductor surface damage produced by ruby lasers, J. Appl. Phys. 36 (1965) 3688–3689, https://doi.org/10.1063/1.1703071.
[2] J. Bonse, S. Gräf, Maxwell meets marangoni - A review of theories on laser-induced periodic surface structures, Laser & Photonics Reviews 14 (2020) 2000215, https://doi.org/10.1002/lpor.202000215.
[3] J. Heitz, E. Ahrenholz, D. Bäuerle, R. Sauerbrey, H.M. Phillips, Femtosecond excimer-laser-induced structure formation on polymers, Appl. Phys. A 59 (1994) 289, https://doi.org/10.1007/BF00348232.
[4] O. Varlamova, J. Reif, Evolution of femtosecond laser induced surface structures at low number of pulses near the ablation threshold, J. Laser Micro/Nanoeng. 8 (2013) 300, https://doi.org/10.2961/jlmn.2013.03.0019.
[5] S. Hohm, A. Rosenfeld, J. Krüger, J. Bonse, Area dependence of femtosecond laser induced periodic surface structures for varying band gap materials after double pulse excitation, Appl. Surf. Sci. 278 (2013) 7–12, https://doi.org/10.1016/j.apsusc.2012.10.188.
[6] T. Apostolova, B. Obreshkov, I. Gnilitskyi, Ultrafast energy absorption and photoexcitation of bulk plasmon in crystalline silicon subjected to intense near-infrared ultrashort laser pulses, Appl. Surf. Sci. 519 (2020) 146087, https://doi.org/10.1016/J.APSUSC.2020.146087.
[7] I. Gnilitskyi, V. Gruzdev, N.M. Bulgakova, T. Mocek, L. Orazi, Mechanisms of high-regularity periodic structuring of silicon surface by sub-MHz repetition rate ultrashort laser pulses, Applied Physics Letters 109 (14) (2016) 143101, https://doi.org/10.1063/1.4963784.
[8] I. Gnilitskyi, T.J.Y. Derrien, Y. Levy, N.M. Bulgakova, Mocek T, L. Orazi, High-speed manufacturing of highly regular femtosecond laser-induced periodic surface structures: physical origin of regularity, Sci. Rep. 7 (2017) 8485, https://doi.org/10.1038/s41598-017-08788-z.

[9] Y. Fuentes-Edfuf, A. Sanchez-Gil, C. Florian, V. Giannini, J. Solis, J. Siegel, Surface plasmon polaritons on rough metal surfaces: role in the formation of laser-induced periodic surface structures, ACS Omega 4 (4) (2019) 6939–6946, https://doi.org/10.1021/acsomega.9b00546.
[10] J. Choi, Y.-G. Shin, K. Cho, W.-S. Chang, S. Chang, S.-H Cho, Improving periodic uniformity of area-type LIPSS on Si wafer using a flat-top beam femtosecond NIR laser, Japanese J. Appl. Phys. (2023), https://doi.org/10.35848/1347-4065/acd094.
[11] H. Yao, B. Guo, T. Zhang, W. Tao, Photocurrent enhancement of topological insulator by femtosecond laser-controlled surface structure, The European Phys. Journal Plus 138 (6) (2023), https://doi.org/10.1140/epjp/s13360-023-04193-w.
[12] M. Mezera, J. Bonse, G.R.B.E. Römer, Influence of Bulk Temperature on Laser-Induced Periodic Surface Structures on Polycarbonate, Polymers 11 (2019) 1947, https://doi.org/10.3390/polym11121947.
[13] Y. Kotsiuba, I. Hevko, S. Bellucci, I. Gnilitskyi, Bitmap and Vectorial Hologram Recording by Using Femtosecond Laser Pulses, Sci Rep 11 (2021) 16406, https://doi.org/10.1038/s41598-021-95665-5.
[14] O.V. Kuznietsov, G.D. Tsibidis, A.V. Demchishin, A.A. Demchishin, V. Babizhetskyy, I. Saldan, S. Bellucci, I. Gnilitskyi, Femtosecond Laser-Induced Periodic Surface Structures on 2D Ti-Fe Multilayer Condensates, Nanomater 11 (2021) 316, https://doi.org/10.3390/NANO11020316.
[15] I. Gnilitskyi, L. Dolgov, A. Tamm, A.M. Ferraria, K. Diedkova, S. Kopanchuk, Y. Tsekhmister, S. Veiksina, V. Polewczyk, M. Pogorielov, Enhanced osteointegration and osteogenesis of osteoblast cells by laser-induced surface modification of Ti implants, Nanomedicine 62 (2024) 102785, https://doi.org/10.1016/j.nano.2024.102785.
[16] A. Lys, I. Gnilitskyi, E. Coy, M. Jancelewicz, O. Gogotsi, I. Iatsunskyi, Highly regular laser-induced periodic silicon surface modified by MXene and ALD TiO_2 for organic pollutants degradation, Appl. Surf. Sci. 640 (2023) 158336, https://doi.org/10.1016/j.apsusc.2023.158336.
[17] J. Bonse, A. Rosenfeld, J. Krüger, On the role of surface plasmon polaritons in the formation of laser-induced periodic surface structures upon irradiation of silicon by femtosecond-laser pulses, J. Appl. Phys. 106 (2009) 104910, https://doi.org/10.1063/1.3261734.
[18] T. Feng, G. Chen, H. Han, J. Qiao, Femtosecond-Laser-Ablation Dynamics in Silicon Revealed by Transient Reflectivity Change, Micromachines 13 (2022) 14, https://doi.org/10.3390/mi13010014.
[19] J. Sládek, I.M. Mirza, Laser Induced Damage Threshold of Silicon with Native and Artificial SiO_2 Layer, MM Sci. J. 2019 (2019) 3579–3584, https://doi.org/10.17973/MMSJ.2019_12_2019103.
[20] T. Dong, M. Sparkes, C. Durkan, W. O'Neill, Evaluating Femtosecond Laser Ablation of Graphene on SiO_2/Si Substrate, J. Laser Appl. 28 (2016) 022202, https://doi.org/10.2351/1.4944510.
[21] Deutsches Elektronen Synchrotron (DESY). DESY NanoLab, J. large- scale res. facilities 2 (2016) A76, https://doi.org/10.17815/jlsrf-2-140.
[22] T. Apostolova, B. Obreshkov, Femtosecond optical breakdown in silicon, Appl. Surf. Sci. 572 (2022) 151354, https://doi.org/10.1016/j.apsusc.2021.151354.
[23] C. Schinke, P.C. Peest, J. Schmidt, R. Brendel, K. Bothe, M.R. Vogt, I. Kröger, S. Winter, A. Schirmacher, S. Lim, H.T. Nguyen, D. MacDonald, Uncertainty analysis for the coefficient of band-to-band absorption of crystalline silicon, AIP Adv 5 (2015) 067168, https://doi.org/10.1063/1.4923379.
[24] S.A. Sato, Y. Shinohara, T. Otobe, K. Yabana, Phys. Rev. B 90 (2014) 174303, https://doi.org/10.1103/PhysRevB.90.174303.
[25] H. Raether, Surface Plasmons on Smooth and Rough Surfaces and on Gratings (Berlin: Springer), Springer-Verlag, Berlin; New York, 1998.
[26] R.J. Bell, R.W. Alexander Jr, W.F. Parks, G. Kovener, Surface excitations in absorbing media, Opt. Commun. 8 (1973) 147, https://doi.org/10.1016/0030-4018(73)90159-4.
[27] F. Garrelie, J.P. Colombier, F. Pigeon, S. Tonchev, N. Faure, M. Bounhalli, S. Reynaud, O. Parriaux, Evidence of surface plasmon resonance in ultrafast laser-induced ripples, Optics Express 19 (2011) 9035, https://doi.org/10.1364/OE.19.009035.
[28] T.J.Y. Derrien, T.E. Itina, R. Torres, T. Sarnet, M. Sentis, J. Appl. Phys. 114 (2013) 083104, https://doi.org/10.1007/s00339-013-8205-2.
[29] P.N. Terekhin, O. Benhayoun, S.T. Weber, D.S. Ivanov, M.E. Garcia, B. Rethfeld, Influence of surface plasmon polaritons on laser energy absorption and structuring of surfaces, Applied Surface Science 512 (2020) 144420, https://doi.org/10.1016/j.apsusc.2019.144420.
[30] A. Hohenau, A. Drezet, M. Weissenbacher, F R Aussenegg, J R Krenn, Effects of damping on surface-plasmon pulse propagation and refraction, Phys. Rev. B 78 (155405) (2008), https://doi.org/10.1103/PhysRevB.78.155405.
[31] F. Garrelie, et al., Evidence of surface plasmon resonance in ultrafast laser-induced ripples, Opt. Express 19 (2011) 9035–9043, https://doi.org/10.1364/OE.19.009035.
[32] G. Miyaji, W. Kobayashi, K. Miyazaki, Reflectivity change in nanoscale modification of DLC film with femtosecond laser pulses, J. Laser Micro Nanoeng 2 (2007) 146, https://doi.org/10.2961/jlmn.2007.02.0008.
[33] S. Höhm, A. Rosenfeld, J. Krüger, J. Bonse, Laser-induced periodic surface structures on titanium upon single-and two-color femtosecond double-pulse irradiation, Optics Express (2015) 25959, https://doi.org/10.1364/OE.23.025959.